J|A|C|S
ARTICLES

A Nanostructure Made of a Bacterial Noncoding RNA

Bastien Cayrol,[†] Claude Nogues,[‡] Alexandre Dawid,[†] Irit Sagi,[‡] Pascal Silberzan,[†] and Hervé Isambert[*,†]

Institut Curie, Research Division, CNRS UMR 168, Paris 75248, France, and The Department of Structural Biology, Weizmann Institute of Science, Rehovot, Israel

Received July 21, 2009; E-mail: herve.isambert@curie.fr

Abstract: Natural RNAs, unlike many proteins, have never been reported to form extended nanostructures, despite their wide variety of cellular functions. This is all the more striking, as synthetic DNA and RNA forming large nanostructures have long been successfully designed. Here, we show that DsrA, a 87-nt noncoding RNA of *Escherishia coli*, self-assembles into a hierarchy of nanostructures through antisense interactions of three contiguous self-complementary regions. Yet, the extended nanostructures, observed using atomic force microscopy (AFM) and fluorescence microscopy, are easily disrupted into >100 nm long helical bundles of DsrA filaments, including hundreds of DsrA monomers, and are surprisingly resistant to heat and urea denaturation. Molecular modeling demonstrates that this structural switch of DsrA nanostructures into filament bundles results from the relaxation of stored torsional constraints and suggests possible implications for DsrA regulatory function.

Biological structures and processes, as well as their regulation, rely on specific interactions between biomolecular components of the cell. While the main functions of protein−protein, DNA−protein, and RNA−protein interactions have long been recognized, the full extent of RNA−RNA interactions has only recently begun to emerge with the discovery of numerous noncoding RNAs in living cells.

Yet, simple RNA−RNA interactions are not known to promote extended natural RNA self-assemblies, even though RNA homodimers and even hexamers[1] have been reported. It is in sharp contrast with the many examples of large supramolecular structures made of proteins, such as microtubules or virus capsids.

In fact, the apparent lack of natural RNA self-assemblies is all the more surprising, as many large artificial nanostructures made of DNA[2−17] or RNA[18−21] have been successfully designed, using Watson−Crick pairing rules or tertiary RNA−RNA motif interactions. In addition, elaborate switchable DNA/RNA molecular systems and nanodevices have even been rationally designed. Hence, in principle, the ability to self-assemble could also be used by natural RNAs, in addition to the already wide variety of known functions they carry out in the cell.

DsrA Nanostructure Predictions and Polyacrylamide Gel Electrophoresis (PAGE) Evidence. DsrA is an 87-nt noncoding RNA of *E. coli* with regulatory properties.[22−28] While conflict-

[†] CNRS UMR 168.

[‡] Weizmann Institute of Science.

(1) Chen, C.; Zhang, C.; Guo, P. *RNA* **1999**, *5*, 805–18.

(2) Yang, X.; Wenzler, L. A.; Qi, J.; Li, X.; Seeman, N. C. *J. Am. Chem. Soc.* **1998**, *120*, 9779–86.

(3) Winfree, E.; Liu, F.; Wenzler, L. A.; Seeman, N. C. *Nature* **1998**, *394*, 539–44.

(4) Mao, C.; sun, W.; Seeman, N. C. *J. Am. Chem. Soc.* **1999**, *121*, 5437–43.

(5) Feng, L.; Park, S. H.; Reif, J. H.; Yan, H. *Angew. Chem., Int. Ed.* **2003**, *42*, 4342–6.

(6) Yan, H.; LaBean, T.; Feng, L.; Reif, J. H. *Proc. Natl. Acad. Sci. U.S.A.* **2003**, *100*, 8103–8.

(7) Rothemund, P.W. K.; Ekani-Nkodo, A.; Papadakis, N.; Kumar, A.; Kuchnir Fygenson, D.; Winfree, E. *J. Am. Chem. Soc.* **2004**, *126*, 16344–52.

(8) Rothemund, P. W. K.; Papadakis, N.; Winfree, E. *PLoS Biol.* **2004**, *2*, e424.

(9) Chelyapov, N.; Brun, Y.; Gopalkrishnan, M.; Reishus, D.; Shaw, B.; Adleman, L. *J. Am. Chem. Soc.* **2004**, *126*, 13924–5.

(10) Ding, B.; Sha, R.; Seeman, N. C. *J. Am. Chem. Soc.* **2004**, *126*, 10230–1.

(11) Shih, W. M.; Quispe, J. D.; Joyce, G. F. *Nature* **2004**, *427*, 618–21.

(12) Liu, H.; Chen, Y.; He, Y.; Ribbe, A. E.; Mao, C. *Angew. Chem., Int. Ed.* **2006**, *45*, 1942–5.

(13) Ding, B.; Seeman, N. C. *Science* **2006**, *314*, 1583–5.

(14) Schulman, R.; Winfree, E. *Proc. Natl. Acad. Sci. U.S.A.* **2007**, *104*, 15236–41.

(15) He, Y.; Ye, T.; Su, M.; Zhang, C.; Ribbe, A. E.; Jiang, W.; Mao, C. *Nature* **2008**, *452*, 198–201.

(16) Yin, P.; Choi, H. M. T.; Calvert, C. R.; Pierce, N. A. *Nature* **2008**, *451*, 318–22.

(17) Yin, P.; Hariadi, R. F.; Sahu, S.; Choi, H. M. T.; Park, S. H.; Labean, T. H.; Reif, J. H. *Science* **2008**, *321*, 824–6.

(18) Jaeger, L.; Leontis, N. B. *Angew. Chem., Int. Ed.* **2000**, *39*, 2521–24.

(19) Chworos, A.; Severcan, I.; Koyfman, A. Y.; Weinkam, P.; Oroudjev, E.; Hansma, H. G.; Jaeger, L. *Science* **2004**, *306*, 2068–72.

(20) Shu, D.; Moll, W.-D.; Deng, Z.; Mao, C.; Guo, P. *Nano Lett.* **2004**, *4*, 1717–23.

(21) Nasalean, L.; Baudrey, S.; Leontis, N. B.; Jaeger, L. *Nucleic Acids Res.* **2006**, *34*, 1381–92.

(22) Sledjeski, D.; Gottesman, S. *Proc. Natl. Acad. Sci. U.S.A.* **1995**, *92*, 2003–7.

(23) Sledjeski, D. D.; Gupta, A.; Gottesman, S. *EMBO J.* **1996**, *15*, 3993–4000.

(24) Muffler, A.; Traulsen, D. D.; Fischer, D.; Lange, R.; Hengge-Aronis, R. *J. Bacteriol.* **1997**, *179*, 297–300.

(25) Lease, R. A.; Cusick, M. E.; Belfort, M. *Proc. Natl. Acad. Sci. U.S.A.* **1998**, *95*, 12456–61.

(26) Majdalani, N.; Cunning, C.; Sledjeski, D.; Elliott, T.; Gottesman, S. *Proc. Natl. Acad. Sci. U.S.A.* **1998**, *95*, 12462–7.

(27) Sledjeski, D. D.; Whitman, C.; Zhang, A. *J. Bacteriol.* **2001**, *183*, 1997–2005.

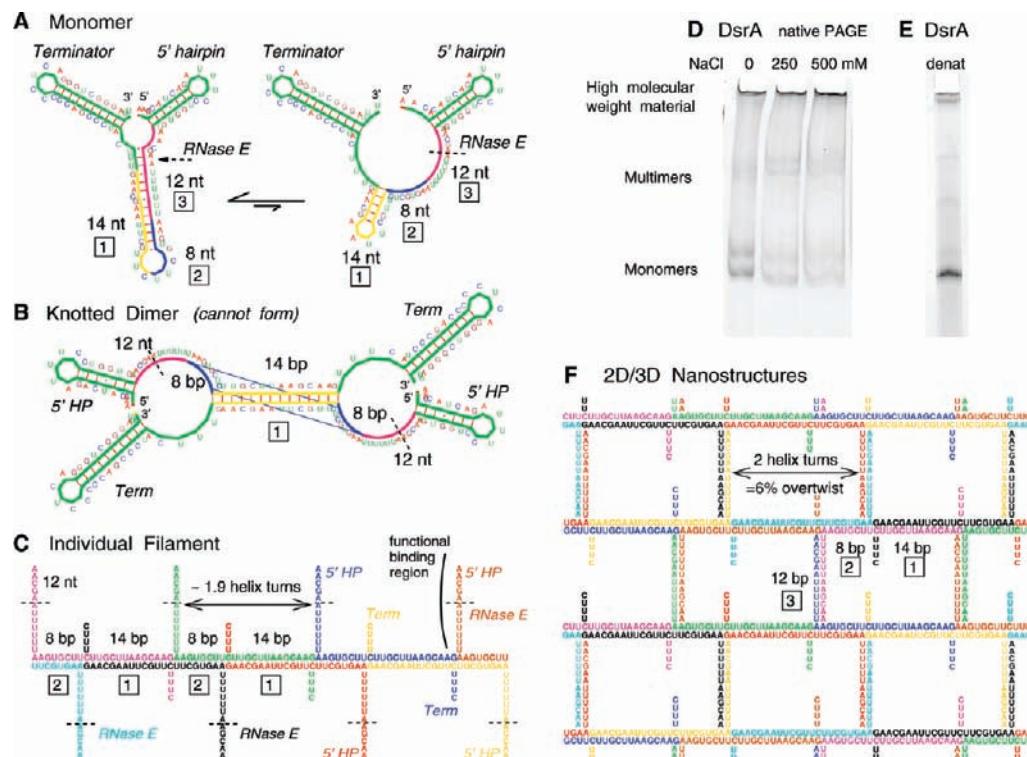(28) Repoila, F.; Gottesman, S. *J. Bacteriol.* **2001**, *183*, 4012–23.

Figure 1. DsrA self-assembly prediction and PAGE evidence. (A) DsrA monomer structures with three contiguous self-complementary regions highlighted, 14-nt (yellow), 8-nt (blue), and 12-nt (magneta). (B) DsrA knotted dimer with both 14-bp and 8-pb duplexes cannot form for topological reasons (see Material and Methods in Supporting Information and ref 31). (C) Predicted DsrA filaments with coaxial stacking of 14-bp and 8-bp duplexes from successive self-assembled DsrA monomers (5′ and terminator hairpins are not shown). DsrA functional binding region interacting with target mRNAs and Hfq protein (see Figure S1) and including an RNase E cleavage site (dashed line) is radially exposed from DsrA filaments. (D) Native PAGE of DsrA transcript under increasing salt concentration. (E) Denaturing PAGE of DsrA transcript. (F) Predicted nanostructure of laterally interacting DsrA filaments through many weak 12-bp bridging duplexes (5′ and terminator hairpins are not shown).

ing results have been published concerning its folded secondary structure,[25,26,29] the spontaneous formation of DsrA dimers has also been reported.[30] This prompted us to look for potential regions promoting DsrA intermolecular interaction.

Using RNA folding and interaction prediction tools,[31] we readily identified three contiguous self-complementary antisense regions in DsrA ncRNA sequence (Figure 1A and Supporting Information Figure S1).

The main two regions with the strongest self-complementary associations are a 14-nt region, 5′-CUUGCUUAAGCAAG-3′, able to form a 14-bp Watson−Crick duplex, immediately preceded by a second 8-nt region, 5′-AAGUGCUU-3′, forming two central GU pairs. Yet, the contiguous locations of these two self-complementary regions along the DsrA sequence was expected to preclude the formation of fully paired DsrA dimers, with both 8-bp and 14-bp duplexes simultaneously formed, Figure 1B, because the corresponding knotted dimer cannot form for topological reasons (see Material and Methods in the Supporting Information and ref 41). Instead, we anticipated that DsrA transcripts could in fact self-associate and form long double-stranded RNA helices by coaxially stacking contiguous 8-bp and 14-bp duplexes from successive DsrA molecules (Figure 1C).

Indeed, performing simple PAGE separations, we noticed that up to 30−50% of in vitro DsrA transcripts hardly migrate under

typical electrophoretic conditions, Figure 1D. Although this high molecular weight material is remarkably resistant to heat and urea denaturation, Figure 1E, we could rule out that it might come from read-through in vitro transcription using blunt PCR fragments for in vitro transcription by T7 or *E. coli* RNA polymerases. In addition, heat renaturation under increasing salt concentration was found to progressively convert low molecular weight bands (DsrA monomers, dimers, ...) into the same hardly migrating band, Figure 1D. The ability of the predicted minimal sequence of 8-nt + 14-nt self-complementary regions to promote DsrA self-assembly was also directly confirmed using the corresponding 22-nt synthetic RNA fragment[32] whereas the 8-nt or the 14-nt regions alone did not show any sign of self-assembly, as expected.

In fact, further analysis of DsrA middle region (in-between its 5′end hairpin and 3′end terminator hairpin, Figures 1A and S1) shows that it also contains a self-complementary sequence, which might possibly form a third duplex with two CU mismatches, 5′-AACGAAUUUUUU-3′, Figures 1A and S1. While the corresponding binding energy, estimated as 2−4 kcal/mol,[33,31] is unlikely to yield isolated DsrA dimers in solution, the addition of many of these weak 12-bp duplexes is expected to induce efficient lateral interactions between individual DsrA filaments, self-assembled from the stronger 8-bp and 14-bp duplexes. The resulting DsrA 2D/3D nanostructures, Figure 1F, may thus provide strong local concentration enhance-

(29) Lease, R. A.; Belfort, M. *Proc. Natl. Acad. Sci. U.S.A.* **2000**, *97*, 9919–24.
(30) Lease, R. A.; Woodson, S. A. *J. Mol. Biol.* **2004**, *344*, 1211–23.
(31) Xayaphoummine, A.; Bucher, T.; Isambert, H. *Nucleic Acids Res.* **2005**, *33*, W605–10.
(32) Cayrol, B.; Geinguenaud, F.; Lacoste, J.; Busi, F.; Le Derout, J.; Pietrement, O.; Le Cam, E.; Regnier, P.; Lavelle, C.; Arluison, V. *RNA Biol.* 2009 Oct 7; 6(4) (Epub ahead of print).
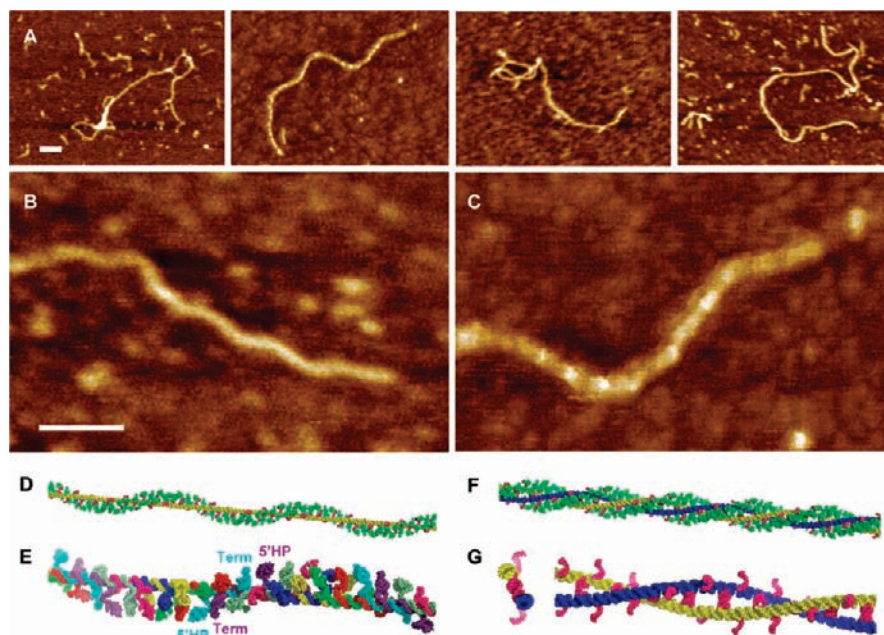(33) Markham, N. R.; Zuker, M. *Nucleic Acids Res.* **2005**, *33*, W577–81.

Figure 2. DsrA filament self-assembly. (A) AFM pictures of DsrA transcript: traditional dried sample preparation on mica (see Material and Methods in Supporting Information). (B, C) Magnification of two characteristic longitudinal modulations with (B) 50 ± 5 nm period and (C) 23 ± 5 nm period. (D) Structural model using pymol[40] of a single DsrA filament with a lefthanded helical decoration from dangling 5′ and 3′ hairpins (green). (E) One left-handed helical turn (~50 nm) with different colors for each successive DsrA molecule. (F) Structural model of two laterally interacting DsrA filaments (yellow and blue) with a left-handed helical decoration from dangling 5′ and 3′ hairpins (green). (G) Cross section (left) and one left-handed (super) helical turn (right) of two laterally interacting DsrA filaments with 12-bp bridging duplexes (magenta). Unpaired 12-nt self-complementary regions are radially exposed (magenta), hence, favoring further lateral accretion processes to occur and eventually larger DsrA self-assembly bundles to form, see main text. 5′ and 3′ hairpins are not shown for clarity. Scale bars: 50 nm.

ments enabling the formation of weakly paired 12-bp duplexes with possible implication for DsrA degradation and regulatory functions (see Discussion).

The actual supramolecular structures of DsrA self-assemblies were then investigated using AFM and fluorescence microscopy techniques.

AFM Observation of Robust Filamentous Self-Assemblies. Traditional AFM imaging of dry deposited samples on freshly cleaved mica readily shows >100 nm-long robust filamentous structures, regarding salt and spreading conditions (see Material and Methods in Supporting Information). Although the AFM technique is not able to resolve the diameters of individual double stranded DNA or RNA helices (2−2.5 nm), we could nonetheless identify different DsrA filamentous self-assemblies from their different longitudinal modulations, Figure 2B,C.

In particular, a thin periodic undulation (period 50 ± 5 nm) is observed on typically 10% of filamentous assemblies, Figure 2B. This pattern closely corresponds to the expected modulation from the molecular model of a single self-assembled DsrA filament, Figure 2D, owing to the ~40° rotation of the 5′ and 3′ hairpins from successive DsrA monomers along a single DsrA filament. Indeed, 8 + 14 = 22bp corresponds to about 1.9 turns of dsRNA helix in solution with ~11.7 bp per helical turn,[34−36] which leads to a left-handed helical decoration with ~50 nm pitch around the expected right-handed dsRNA helix, Figure 2E (see Material and Methods). Yet, typical filamentous self-assemblies are thicker with little or no visible modulation

pattern, suggesting that they are in fact bundles of interacting filaments. In particular, a symmetric modulation pattern with about half the period of single filament modulation (23 ± 5 nm) is also observed, Figure 2D, which may correspond to the expected left-handed helical winding of two laterally interacting filaments, due to the formation of multiple 12-bp bridging duplexes, as depicted on Figure 2F,G. In addition, laterally interacting DsrA filaments are also expected to easily form branched filamentous structures caused by T-junction defects, as typically observed, Figure 2A.

We also studied DsrA self-assembly by AFM in buffer, Figure 3 (see Material and Methods). While single filaments and twisted filament bundles can be imaged in buffer, they do not adhere strongly to the surface or are destroyed after a few scanning images, as comparison between Figure 3 panels A and B shows. Yet, we observed some *flat* parallel filament bundles, which were found to adhere more tightly to the surface under buffer, than the more abundant helical filament bundles (Figure 3). These parallel arrangements of individual filaments could be imaged and analyzed in detail. Quantitative analysis of their height profiles as well as lateral distances between filaments, Figure 3C,D, largely confirm the proposed nanostructure model of parallel laterally interacting filaments, Figure 1F (see Figure 3 caption for details).

Further evidence demonstrates, however, that these bundles including a few DsrA filaments actually result from the mechanical disruption of much larger but fragile anisotropic DsrA nanostructures during AFM sample preparation.

DsrA Forms Extended but Fragile Nanostructures. Direct observation showing that DsrA initially self-assemble into much larger and more complex nanostructures was first established by fluorescence microscopy, in solution, using either SYBRgreen II staining dye (Figure 4A, inset) or producing fluorescent DsrA

(34) Conte, M. R.; Conn, G. L.; Brown, T.; Lane, A. N. *Nucleic Acids Res.* **1997**, *25*, 2627−34.
(35) Clore, G. M.; Gronenborn, A. M.; McLaughlin, L. W. *Eur. J. Biochem.* **1985**, *151*, 153−65.
(36) Arnott, S.; Chandrasekaran, R.; Millane, R. P.; Park, H. S. *Biophys. J.* **1986**, *49*, 3−5.
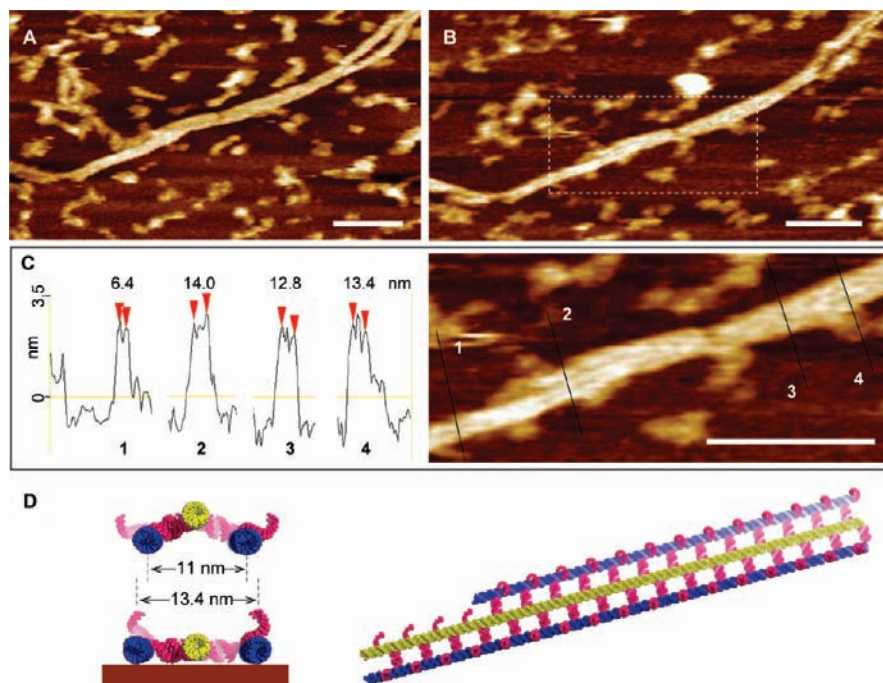
Figure 3. AFM imaging of parallel, laterally interacting DsrA filaments in buffer. (A,B) Flat bundles of parallel, laterally interacting filaments are found to adhere more tightly to the surface than the more abundant single filaments and helical filament bundles, which are easily damaged by the scanning tip in buffer (e.g., the single filament in the top left corner of panel A is heavily damaged in panel B after just a couple of AFM images). Note, that the flat filament bundle is also locally desorbed by the scanning tip (compare the top right corner in panels A and B), see main text. Scale bars = 100 nm. (C) Quantitative height and width profile measurements of these flat parallel filament bundles: height, 3.2 ± 0.2 nm; lateral distance between parallel filaments, 6.7 ± 0.4 nm (i.e., 13.4 ± 0.8 nm measured for three tightly adsorbed parallel filaments, as compared to the ~11 nm for the undeformed predicted structure, panel D and Material and Methods). Scale bar 100 nm. (D) Corresponding model of tightly adsorbed parallel filament bundle, see main text. The 5′ and terminator hairpins are not shown but presumably account for the heights of the profiles (C), which are about 25% higher than a single dsRNA helix diameter (~2.6 nm).

transcripts with 5% Alexa-488 labeled rUTP by T7 in vitro transcription (Figure 4A). Careful handling of DsrA transcripts clearly demonstrates the existence of elongated but fragile fluorescent assemblies in solution that become readily disrupted upon surface adhesion to the glass coverslip, leaving a characteristic micrometer scale pattern as shown on Figure 4A.

These large nanostructures could not be satisfactorily imaged by AFM in buffer, as they do not lie uniformly flat on the surface and are easily scratched by the scanning tip to which they readily stick (by contrast to synthetic DNA or RNA nanostructures designed to be both mechanically stable and compatible with surface adhesion). These large supramolecular self-assemblies are also very fragile to pipeting shear in solution and almost systematically torn to filamentous pieces under usual AFM sample preparations in air, Figure 2, as well as under less gentle handling of DsrA transcript solutions during fluorescence microscopy sample preparation (not shown).

To observe the structural organization of these large self-assemblies at a finer spatial resolution than fluorescence microscopy, we adopted a less disruptive AFM sample preparation by letting the DsrA transcript solution slowly dry (15−20 min) in between a silicon wafer and a glass coverslip (see Material and Methods). Indeed, direct fluorescent observations of the adsorbed nanostructures upon dewetting show that their characteristic micrometer scale pattern (Figure 4A) is left intact by the receding meniscus. This was confirmed by imaging the dry samples under AFMtapping mode, which show the same large, elongated structures, Figure 4B,D, as observed in solution under fluorescence microscopy (Figure 4A), while allowing for progressive zooming and local analysis of the fragile disrupted nanostructures under surface adhesion.

The most regular regions (Figure 4E) from DsrA extended nanostructures (Figure 4D) correspond to smooth 54 ± 5 nm striped patterns (Figure 4F), *parallel* to the elongated direction of the supramolecular self-assembly. These smooth longitudinal stripes also clearly display *perpendicular* striations. The striation period for *undisrupted* stripes is 11.5 ± 2 nm (see quantitative profiles in Figure 4G−I). However, under structural disruption, the ~11 nm striations are observed to coarsen into thicker aggregates, while the underlying longitudinal stripes concomitantly disappear and fuse (see top of Figure 4F and Figure 4G−I). Further accretion process eventually leads to the emergence of regularly spaced coiled-up agregates of increasing sizes, from 30-nm range (Figure 4F top, and Figure 4G−I) to 300-nm range (Figure 4C bottom) and even micrometer range (Figure 4B bottom, also seen by fluorescence, Figure 4A). Such a self-similar-looking (or fractal-like) pattern at different length scales is typically characteristic of an underlying accretion mechanism.

These striking structural patterns and their deformations are in fact consistent with an underlying self-assembly of aligned, laterally interacting DsrA filaments, as initially proposed in Figure 1F and directly observed under buffer in Figure 3. Indeed, the structural model for extended nanostructures of laterally interacting DsrA filaments, Figure 5A, requires that the natural rotation between successive 12-bp bridging duplexes (Figure 2B,D,E) is eliminated through a torsional constraint stored in a ~6% right-handed overtwist of individual DsrA filaments. Such a torsional constraint is expected to be converted for energy minimization into a topologically equivalent helical curvature
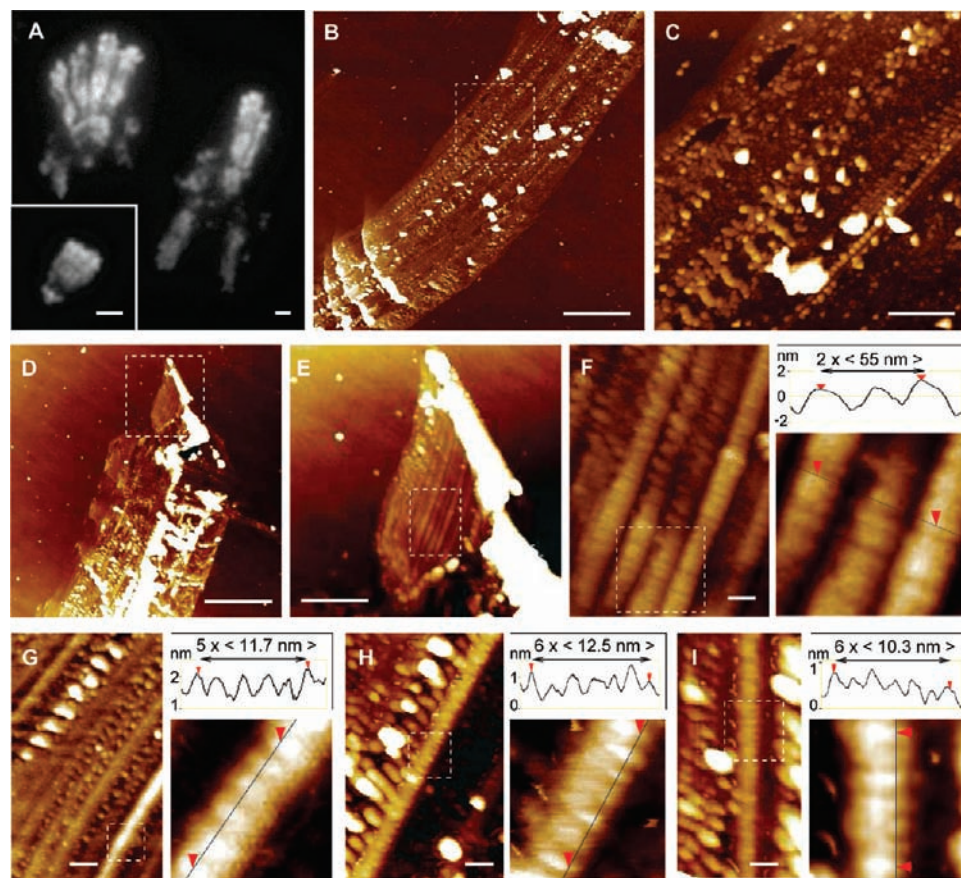
Figure 4. DsrA 2D/3D nanostructures. (A) Fluorescence microscopy pictures of DsrA self-assembly with fluorescent DsrA transcript from T7 RNAPol in vitro transcription (with 5% Alexa-488 labeled rUTP) or with DsrA nonfluorescent transcript from *E. coli* RNAPol in vitro transcription stained by SYBRgreen II (inset). Scale bars = 2 μm. (B−I) AFM pictures of similar disrupted DsrA nanostructures on silicon wafer substrate (see main text and Material and Methods). The long direction of the supramolecular self-assembly is regularly interrupted by *perpendicular* coiled-up aggregates of various sizes, from micrometer range (Figure 4B bottom, also seen by fluorescence, Figure 4A) to 300-nm range (Figure 4C bottom) and even 30-nm range (Figure 4F, top and Figure 4G−I). Such a self-similar-looking (or fractal-like) pattern at different length scales is typically characteristic of an underlying accretion mechanism. (D−F) By contrast, the least disrupted regions of these large DsrA nanostructures correspond to a regular 54 ± 5-nm striped pattern, *parallel* to the elongated direction of the supramolecular self-assembly. (G−I) Undisrupted stripes display also a 11.5 ± 2 nm striation. Scale bars: (A,B and D) = 2 μm, (C and E) = 500 nm, (F−I) = 50 nm.

(or "writhe"[37]) with a 53 ± 5 nm period, as depicted in Figure 5A (see Material and Methods). This is analogous to the linear-supercoiled transition of dsDNA above ∼2% overtwist.[38] Thus, while interacting DsrA filaments are essentially parallel, their collective writhe modulation is expected to lead to a regular striped pattern in the perpendicular direction, Figure 5A. Note that this predicted writhe-induced corrugation is *entirely constrained* by the twist/writhe geometric conversion rule *without any fitting parameter* other than the reported 11.7 bp/turn pitch of dsRNA helix.[34−36] Twist/writhe conversion is thus the most likely structural feature underlying the observed 54 ± 5 nm longitudinal stripes in large, elongated nanostructures, Figures 4D−F. This is further corroborated by the fact that the predicted ∼11 nm striation between every second filaments (Figures 3D and 5A) is also clearly observed along undisrupted stripes (see quantitative profile measurements in Figures 4G−I and 5C,D).

Disruption of DsrA Nanostructures Relaxes Stored Torsional Constraints. The alignment of individual DsrA filaments also explains the mechanical fragility of DsrA 2D/3D anisotropic nanostructures, as local fractures (caused by hydrodynamic shear, surface adhesion, or other changes affect-

ing the 12-bp duplex stability) can readily propagate along the parallel filaments through successive dissociation of the weak 12-bp bridging duplexes. This is predicted to lead to the relaxation of the stored torsional constraints into characteristic structural rearrangements depicted in Figure 5B. Indeed, pairs or small bundles of broken DsrA filaments remaining under mutual lateral interactions are expected to mechanically relax into left-handed helicoidal bundles, as illustrated in Figure 2F,G. By contrast, the global helical winding constraint for unbroken DsrA filaments imposes, in this case, an opposite L-twist/R-writhe cancellation, as depicted in Figure 5B.

These structural predictions (Figure 5A,B) are in good agreement with the different characteristic patterns observed at the onset and early steps of the fragmentation of large DsrA nanostructures, as depicted in Figure 5D. Although still in one piece, the extended nanostructure is invaded by internal "cracks" along its laterally interacting filaments. At the same time, local disruptions of 12bp duplexes are transmitted *across* tens to hundreds laterally interacting filaments, along the direction of the ∼50 nm stripes, as observed in Figures 4G−I and 5D. Such mesoscopic correlation length scales provide a direct structural basis for the observed fragility of DsrA nanostructures, due to their stored torsional constraints. In addition, the relaxation of built-in mechanical constraints stored in DsrA extended nano-

(37) Fuller, F. B. *Proc. Natl. Acad. Sci. U.S.A.* **1971**, *68*, 815–9.
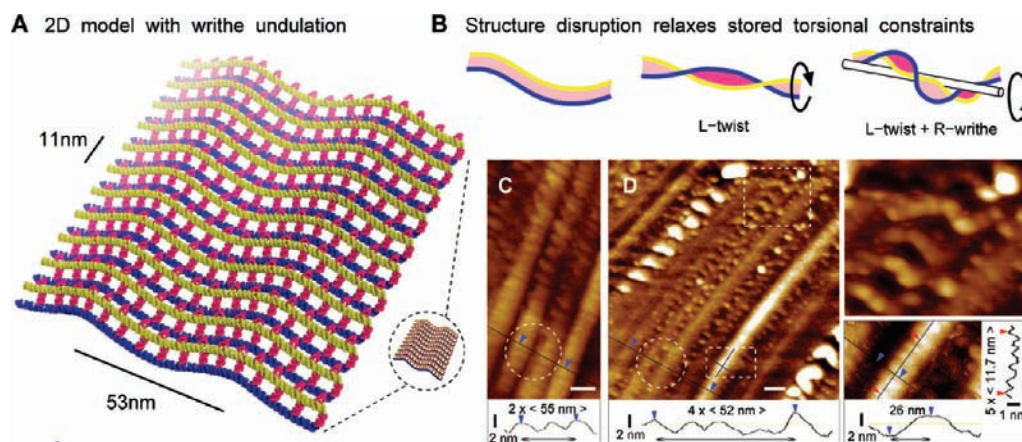(38) Marko, J. F.; Siggia, E. D. *Phys. Rev. E* **1995**, *52*, 2912–2938.

Figure 5. 2D/3D model of extended DsrA nanostructure. (A) Structural model of 2D DsrA self-assembly (see Material and Methods). Individual DsrA filaments (blue and yellow) interact laterally by forming many weak 12-bp bridging duplexes (magenta), which requires that their natural left-handed rotation (Figure 2D,E) is eliminated by an opposite ∼6% right-handed overtwist. This is, however, converted for energy minimization into a topologically equivalent helical curvature (or "writhe") with a 53 ± 5 nm period producing a regular striped pattern (perpendicular to the aligned DsrA filaments) (see also main text, Figure 3, and Material and Methods) (5′ and 3′ hairpins are not shown for clarity). (B) Relaxation of stored torsional constraint by disruption of regular DsrA nanostructures: broken pairs of interacting filaments relax into left-handed superhelical conformations, "L-twist" (Figure 2F,G) and further cluster into larger filament bundles while the global helical winding constraint for pairs of unbroken filaments produces a characteristic local modulation pattern, due to an opposite twist/writhe cancellation, "L-twist + R-writhe". (C, D) Corresponding AFM observation showing different characteristic patterns consistent with the extended nanostructure model (A) and its mechanical disruption (B) (see main text).

structures (Figure 5B) is also consistent with their observed global fragmentation, leaving only few intermediate sized pieces. This is analogous to the well-known fragmentation property of "tempered" (safety) glass, which also stores *internal mechanical constraints* and shatters, as a result, into small pieces without leaving (dangerous) intermediate sized pieces.

Discussion

We report, in this paper, self-assembly predictions, experimental evidence and detailed structural models demonstrating the formation and disruption of a hierarchy of nanostructures made by a small noncoding RNA of *E. coli*. Three contiguous self-complementary regions along the DsrA sequence are responsible for the formation of these novel nanostructures, whose unbounded growth *in vitro* can even exceed the size of *E. coli* itself.

Interestingly, the self-assembly of DsrA nanostructures enables the collective formation of weakly paired 12-bp duplexes that overlap both with the cleavage site (5′-AAUUU-3′) of a single-strand endoribonuclease (RNase E) and the functional region of DsrA, that is known to bind several target mRNAs, such as *rpoS*[25,26] and *hns*,[25] as well as an Sm-like RNAbinding protein cofactor, Hfq,[24,27,30] Figure S1. So, unlike protein filaments or microtubules, which function as structural scaffolds and molecular rails for protein motors, the self-assembly and mechanical properties of DsrA nanostructures might instead be coupled to the degradation and regulatory functions of this noncoding RNA.

Indeed, DsrA degradation and regulatory functions have been reported to be directly coupled under temperature stress[28] and Hfq cofactor activity.[27] Yet, such a functional coupling between seemingly antagonistic degradation and regulatory functions involving the same singlestranded AU-rich region (Figure S1) likely entails a fine-tuned structural control of DsrA, which has remained elusive so far. In this regard, the formation of the weak 12-bp duplexes and the resulting fragility of DsrA anisotropic nanostructures may actually provide a useful platform for the control of DsrA regulatory functions under stress. In particular, the relaxation of stored torsional constraints through an induced

structural switch of DsrA nanostructures is expected to trigger the sudden exposition of a large number of single-stranded functional binding sites, previously stored as weakly paired 12-bp duplexes.

Such a requirement for a large number of DsrA transcripts is corroborated, in particular, by the fact that DsrA should bind with a one-to-one stoichiometry to its target mRNAs, *rpoS* and *hns*, which are both in the range of 30−50 transcript copies per bacterium cell, when significantly expressed[39] (https://asap.ahabs.wisc.edu/asap/experiment data.php). It implies that the DsrA transcript copy number should be of the order of 60−100 transcripts per bacterium or above to efficiently regulate the translation of its available *rpoS* and *hns* mRNA targets. This corresponds to an in vivo DsrA concentration of about 0.1−0.15 μM, which is in the typical range of concentrations we have used to image DsrA nanostructures in vitro in this study (see Material and Methods). All in all, this suggests that DsrA nanostructures likely form in vivo and derive their biological functions from the large-scale relaxation of their built-in torsional constraints.

While this hypothesis will require careful functional studies, the formation and structural details of DsrA nanostructures reported here provide the basis of an alternative structural framework to analyze how this bacterial regulatory RNA might actually operate in cells.

Furthermore and beyond premature speculations about the general importance or specific functions of other RNA nanostructures, it would be very surprising that DsrA remains the only natural RNA with self-assembly properties. Hence, nanostructures, that have been so successfully designed from synthetic DNA[2−17] and RNA[18−21] sequences, may have their functional counterparts in nature as well, thereby extending further the striking versatility of nucleic acids in cells.

(39) Allen, T. E.; Herrgard, M. J.; Liu, M.; Qiu, Y.; Glasner, J. D.; Blattner, F. R.; Palsson, B. O. *J. Bacteriol.* **2003**, *185*, 6392–9.
(40) DeLano, W. L. *The PyMOL Molecular Graphics System*; DeLano Scientific: Palo Alto, CA, 2002. (http://www.pymol.org).
(41) Isambert, H. *Methods* **2009**, *49*, 189–196.

Supporting Information Available: Materials and Methods section; additional figures. This material is available free of charge via the Internet at http://pubs.acs.org.

JA906076E